Journal of Computer-Aided Molecular Design **19:** 17–31, 2005.
DOI 10.1007/s10822-005-0098-5

Free energy perturbation approach to the critical assessment of selective cyclooxygenase-2 inhibitors

Hwangseo Park* & Sangyoub Lee*
School of Chemistry and Molecular Engineering, and Center for Molecular Catalysis, Seoul National University, Seoul 151-747, South Korea

Received 7 October 2004; accepted in revised form 29 December 2004

Key words: cyclooxygenase inhibitors, force field design, free energy perturbation, molecular dynamics simulation, selectivity

Summary

The discovery of selective cyclooxygenase-2 (COX-2) inhibitors represents a major achievement of the efforts over the past few decades to develop therapeutic treatments for inflammation. To gain insights into designing new COX-2-selective inhibitors, we address the energetic and structural basis for the selective inhibition of COX isozymes by means of a combined computational protocol involving docking experiment, force field design for the heme prothetic group, and free energy perturbation (FEP) simulation. We consider both COX-2- and COX-1-selective inhibitors taking the V523I mutant of COX-2 to be a relevant structural model for COX-1 as confirmed by a variety of experimental and theoretical evidences. For all COX-2-selective inhibitors under consideration, we find that free energies of binding become less favorable as the receptor changes from COX-2 to COX-1, due to the weakening and/or loss of hydrogen bond and hydrophobic interactions that stabilize the inhibitors in the COX-2 active site. On the other hand, COX-1-selective oxicam inhibitors gain extra stabilization energy with the change of residue 523 from valine to isoleucine because of the formations of new hydrogen bonds in the enzyme-inhibitor complexes. The utility of the combined computational approach, as a valuable tool for *in silico* screening of COX-2-selective inhibitors, is further exemplified by identifying the physicochemical origins of the enantiospecific selective inhibition of COX-2 by α-substituted indomethacin ethanolamide inhibitors.

Introduction

Cyclooxygenases (COXs), also known as prostaglandin H2 synthases, are a membrane-bound peroxidase with a heme prothetic group conferring the enzymatic activity [1]. COX-1 and COX-2 are two isoforms of COX, which catalyze the first two steps in the biosynthesis of prostaglandins that contribute to a variety of physiological functions [2]. Although the two isozymes share the identical catalytic mechanism, COX-2 is known to be responsible for prostaglandin formation in inflammation whereas COX-1 performs a number of homeostatic functions such as maintaining normal gastric mucosa, influencing renal blood flow, and platelet aggregation [3]. For this reason, considerable efforts have been made over the past decade to find selective COX-2 inhibitors and thereby to develop a new generation of non-steroidal anti-inflammatory drugs (NSAIDs). Besides the involvement in inflammation, recent studies have shown that COX-2 plays a direct role in many human pathologies including various cancers [4–7], pain and fever [8], and Alzheimer's disease [9, 10], offering a perspective for further use of its selective inhibitors.

Three-dimensional structures of the two isozymes were reported in both free and ligand-bound forms [11–19]. The structural alignment

*Correspondence may be addressed to either author. Fax: +82-2-889-1568; E-mails: hwangseo@snu.ac.kr; sangyoub@snu.ac.kr

shows that they are structurally homologous and quite superimposable with the C_α rmsd of 0.47 Å [14], which is not surprising since they have sequence identity higher than 60%. Both of the COX isoforms are dimeric, and each monomer consists of three structural domains [20]: the N-terminal epidermal growth factor domain, a membrane binding domain, and a large C-terminal globular catalytic domain containing the heme binding site. As shown in Figure 1, the active sites of COX-1 and COX-2 share a sequence identity higher than that of the whole proteins, which is responsible for the difficulty in designing a selective inhibitor. In the sequence alignment of the two COX isoforms, much attention has been paid to the residue difference at position 523 because the substitution of valine in COX-2 for isoleucine in COX-1 leads to the increase of the accessible space in the active site [21]. This substitution is believed to have an effect of opening up a small side pocket that may be important in the binding of selective COX-2 inhibitors. Indeed, the importance of the position 523 as a discrimination factor between the two COX isoforms was well-appreciated in the mutagenesis studies, which showed that the single amino acid substitution of isoleucine at position 523 for valine made COX-2 act like COX-1 in enzyme assay and *vice versa* [22–24].

Since the discovery and characterization of COX-2 isozyme, more than a thousand of its inhibitors have been reported in the literature with structural diversity [25–43]. Now, at least two molecules (celecoxib and rofecoxib) are in clinical use as anti-inflammatory and analgesic drugs. Many computational studies have also been reported within a variety of theoretical frameworks [44–55]. Although most of them were focused on rationalizing the relative potencies of various COX-2 inhibitors without a rigorous consideration of structural origins for the reduced binding affinities in COX-1, Price and Jorgensen provided a rationale for the selective inhibition of COX-2 by celecoxib from Monte Carlo simulations [47]. Based on the free energy simulations, they showed that the decrease in binding affinity of celecoxib in going from COX-2 to COX-1 could be attributed to the unfavorable steric contact between the inhibitor sulfonamide oxygen and the terminal methyl group of Ile523. Very recently, Soliva et al. performed free energy perturbation (FEP) calculations based on molecular dynamics (MD) simulation to address the inhibition mechanism of COX-2, and displayed the utility of the MD–FEP method in explaining the relative potencies of structurally related inhibitors and their size effects on the flexibility of the active site [48].

```
COX1   1 MSRQSISLRFPLLLLLLSPSPVFSADPGAPAPVNPCCYYPCQHQGICVRFGLDRYQCDCTRTGYSGPNCTIPEIWTWLRTTLRPSPSFIHFMLTHGRWLW 100
COX2     ---------------MLFRAVLLCAALGLSQAANPCCSNPCQNRGECMSTGFDQYKCDCTRTGFYGENCTTPEFLTRIKLLLKPTPNTVHYILTHFKGVW
                         :*  : :: *  *   ..****  ***::* *:  *:*:*:*******: * *** **: * ::  *:*:*  :*::*** : :*

                            120
COX1 101 DFVN-ATFIRDTLMRLVLTVRSNLIPSPPTYNIAHDYISWESFSNVSYYTRILPSVPRDCPTPMGTKGKKQLPDAEFLSRRFLLRRKFIPDPQGTNLMFA 199
COX2     NIVNNIPFLRSLIMKYVLTSRSYLIDSPPTYNVHYGYKSWEAFSNLSYYTRALPPVADDCPTPMGVKGNKELPDSKEVLEKVLLRREFIPDPQGSNMMFA
         ::**   *:*  :*: *** ** ** ******: : * ***:***:***** ** *  ******* **:*:***:: :  : ****:*******:*:***
           203 207   211-220                                                                  289-295
COX1 200 FFAQHFTHQFFKTSGKMGPGFTKALGHGVDLGHIYGDNLERQYQLRLFKDGKLKYQMLNGEVYPPSVEEAPVLMHYPRGIPPQSQMAVGQEVFGLLPGLM 299
COX2     FFAQHFTHQFFKTDHKRGPGFTRGLGHGVDLNHIYGETLDRQHKLRLFKDGKLKYQVIGGEVYPPTVKDTQVEMIYPPHIPENLQFAVGQEVFGLVPGLM
         **************  * *****: ******* ****: *:**::************:: ******:*::: * * **  ** : *:*********:****

                                                                  355                             385
COX1 300 LYATIWLREHNRVCDLLKAEHPTWGDEQLFQTARLILIGETIKIVIEEYVQQLSGYFLQLKFDPELLFGAQFQYRNRIAMEFNQLYHWHPLMPDSFRVGP 399
COX2     MYATIWLREHNRVCDILKQEHPEWGDEQLFQTSRLILIGETIKIVIEDYVQHLSGYHFKLKFDPELLFNQQFQYQNRIASEFNTLYHWHPLLPDTFNIED
         :***************:** *** *********:***************:***:**** ::**********  ****:**** *** *******:**:* :

                                     434
COX1 400 QDYSYEQFLFNTSMLVDYGVEALVDAFSRQPAGRIGGGRNIDHHILHVAVDVIKESRVLRLQPFNEYRKRFGMKPYTSFQELTGEKEMAAELEELYGDID 499
COX2     QEYSFKQFLYNNSILLEHGLTQFVESFTRQIAGRVAGGRNVPIAVQAVAKASIDQSREMKYQSLNEYRKRFSLKPYTSFEELTGEKEMAAELKALYSDID
         *:**::***:* *:*:::*:  :*::*:** ***: ****:   :  **   * :** :: * :******* :******:************: ** ***

           503       513       523-524 530
COX1 500 ALEFYPGLLLEKCHPNSIFGESMIEMGAPFSLKGLLGNPICSPEYWKASTFGGEVGFNLVKTATLKKLVCLNTKTCPYVSFHVPDP-------------- 585
COX2     VMELYPALLVEKPRPDAIFGETMVELGAPFSLKGLMGNPICSPQYWKPSTFGGEVGFKIINTASIQSLICHNVKGCPFTSFNVQDPQPTKTATINASASH
          :*:** **:** :*::****:*:*:*********:*******:*** *********::::**::: *:* * * **: **:* **

COX1 586 -RQEDRPG---VERPPTEL 600
COX2     SRLDDINPTVLIKRRSTEL
          * :*      ::*  ***
```

Figure 1. Alignment of the amino acid sequences of ovine COX isozymes. Asterisks and colons represent the identity and the similarity between the corresponding residues, respectively. Catalytically important amino acids are indicated in red color with their residue numbers above the sequence. This sequence alignment was derived with Clustal W v1.82.

In this contribution, an extensive computational protocol involving docking experiment, force field design for the heme prothetic group, and MD–FEP simulation is applied to address the energetic and structural features relevant to the selective inhibition of COX-2. In order to estimate the relative binding free energy ($\Delta\Delta G_{\text{bind}}$) of a given inhibitor I in COX-1 compared to that in COX-2, we employ a simple thermodynamic cycle as depicted in Figure 2. Here, the V523I mutant of COX-2 is assumed to be a relevant structural model for COX-1 on the basis of the aforementioned experimental and computational evidences. Since the free energy is a state function, the sum of all free energy changes in a thermodynamic cycle is zero. Therefore, $\Delta\Delta G_{\text{bind}}$ can be expressed as

$$\Delta\Delta G_{\text{bind}} = \Delta G_2 - \Delta G_1 = \Delta G_b - \Delta G_u, \quad (1)$$

where ΔG_1 and ΔG_2 refer to the binding free energies of inhibitor I in COX-2 ($\boldsymbol{E_1}$) and COX-1 ($\boldsymbol{E_2}$), respectively, and ΔG_{u} and ΔG_{b} to the free energy changes associated with the virtual transformations of E_1 into E_2 in the resting and inhibitor-bound forms, respectively. We obtain $\Delta\Delta G_{\text{bind}}$ by FEP calculations of ΔG_{u} and ΔG_{b} with molecular dynamics simulations.

Based on this computational strategy, we estimate $\Delta\Delta G_{\text{bind}}$ values for various COX inhibitors shown in Figure 3. The ability to cope with a wide range of inhibitors is the merit of the present FEP calculation against the conventional method in which only the structurally related inhibitors have been considered to elucidate their

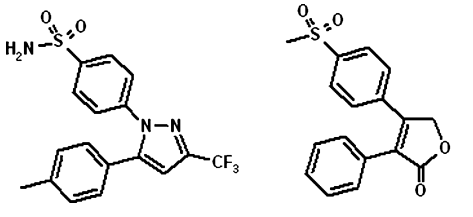

Figure 2. Thermodynamic cycle used in calculating free energy changes in the virtual transformations COX-2 (E_1) into COX-1 (E_2) in the resting (ΔG_{u}) and inhibitor-bound (ΔG_{b}) forms, and the relative binding free energy of inhibitor I in the two isozymes ($\Delta\Delta G_{\text{bind}}$).

Figure 3. Molecular structures of 10 COX inhibitors under investigation. Numbers in parentheses indicate *in vitro* COX-2 selectivity index given by IC_{50} (COX-1) / IC_{50} (COX-2).

relative inhibitory activities. Related with the stereospecificity in enzyme–ligand interaction, it was demonstrated that α-substituted indomethacin ethanolamide (AIE) inhibitors could be transformed from highly selective COX-2 to nonselective inhibitors by the simple inversion of stereochemistry at a single chiral center [56]. Within the present computational framework, we will also address the origins of such a difference in enantiomeric discrimination level between the two COX isoforms.

Computational methods

Docking experiments

The AutoDock 3.0.5 program was used to obtain the starting structures for MD simulation of COX-2-inhibitor complexes. It combines a rapid energy evaluation through precalculated grids of affinity potentials with the Lamarckian genetic algorithm to find suitable binding positions for a ligand on a protein receptor [57]. Although the protein structure has to be fixed, the program allows torsional flexibility of the ligand. The coordinates of the protein atoms were taken from the X-ray crystal structure (PDB entry: 1CX2) reported by Kurumbail et al. [13]. Docking to the COX-2 active site was then carried out using the empirical scoring function that has the following form:

$$\begin{aligned}\Delta G^{\mathrm{aq}}_{\mathrm{bind}} = {} & W_{\mathrm{vdW}} \sum_i \sum_j \left(\frac{A_{ij}}{r_{ij}^{12}} - \frac{B_{ij}}{r_{ij}^{6}} \right) \\ & + W_{\mathrm{hbond}} \sum_i \sum_j E(t) \left(\frac{C_{ij}}{r_{ij}^{12}} - \frac{D_{ij}}{r_{ij}^{10}} \right) \\ & + W_{\mathrm{elec}} \sum_i \sum_j \frac{q_i q_j}{\varepsilon r_{ij}} + W_{\mathrm{tor}} N_{\mathrm{tor}} \\ & + W_{\mathrm{sol}} \sum_i \sum_j (S_i V_j + S_j V_i) \exp\left(-r_{ij}^2 / 2\sigma^2 \right),\end{aligned} \tag{2}$$

where W_{vdW}, W_{hbond}, W_{elec}, W_{tor}, and W_{sol} are weighting factors of van der Waals, hydrogen bond, electrostatic interactions, torsional term, and desolvation energy of inhibitors, respectively. The hydrogen bond term has an additional weighting factor, $E(t)$, representing the angle-dependent directionality. A sigmoidal distance-dependent dielectric function proposed by Mehler et al. [58] was used in computing the interatomic electrostatic interactions between COX-2 and its inhibitors. In the desolvation term, S_j and V_j are the solvation parameter and the fragmental volume of atom j [59], respectively. Of the conformations obtained from 200 independent docking runs, those clustered together have similar binding modes differing by less than 1.5 Å in positional root-mean-square deviation. The most stable configuration of enzyme–inhibitor complex was then selected for further analysis.

Force field design for the heme prothetic group and COX inhibitors

The bonded approach proposed by Hoops et al. [60] was adopted to introduce explicit bonds between the central ferric ion and its ligand atoms. This choice was based on the earlier computational finding that other non-bonded approaches had been sensitive to the electrostatic model used, leading to an undesirable coordination geometry at metal centers [61, 62]. The equilibrium bond lengths and bond angles involving the iron atom were taken from the optimized structure of heme. This geometry optimization was performed at B3LYP/6-31G* level of theory with the Jaguar program [63]. For the force constant parameters involving the ferric ion, we used the values from the Giammona's work [64]. Using the energy-minimized structure, atomic partial charges were derived by using the RESP methodology [65] at RHF/6-31G* level of theory, to be consistent with the standard AMBER force field [66]. All the torsions involving the metal–ligand bonds were set to zero as in the Giammona's work [64]. Other missing force field parameters for heme were estimated from similar chemical species in the AMBER force field database. We derived the potential parameters for all COX inhibitors under investigation by following the same procedure as for the heme prothetic group, which involves the geometry optimization and charge fitting with the RESP method.

Molecular dynamics and FEP calculation

MD simulations of COX-2 in complex with the inhibitors were carried out using the SANDER module of AMBER 7 [67] with the newly developed force field parameters for heme in addition to

those reported by Cornell et al. [66]. As a starting structure, we used the most stable COX-2-inhibitor complex found in the docking simulation. The all-atom models for the enzyme-inhibitor complexes were immersed in rectangular boxes containing about 17,225 TIP3P [68] water molecules. After 1000 cycles of energy minimization to remove the bad steric contacts, we equilibrated the systems beginning with 20 ps equilibration dynamics of the solvent molecules at 300 K. The next step involved equilibration of the solute with a fixed configuration of the solvent molecules consecutively at 10, 50, 100, 150, 200, 250, and 300 K for 5 ps at each temperature. Then, the equilibration dynamics of the entire system was performed at 300 K for 20 ps.

To determine $\Delta\Delta G_{\text{bind}}$ for a given inhibitor in aqueous solution, the free energy changes involved in mutating E_1 (initial state) into E_2 (final state) should be calculated for both unliganded and liganded forms of the receptor protein. Both of the free energy changes can be computed by perturbing the Hamiltonian of the initial state into that of the final state. This transformation is accomplished through a parametrization of terms comprising the interaction potentials of the system with a change of state variable (λ) that maps onto the initial ($\lambda = 0$) and the final ($\lambda = 1$) states. The total free energy change for the mutation from the initial to the final states is then computed by summing the incremental free energy changes over several windows visited by λ as it changes from 0 to 1 [69];

$$\Delta G = G_1 - G_0 = \sum_i (G_{\lambda(i+1)} - G_{\lambda(i)}) = -RT \sum_i \ln\langle \exp - \left[(V_{\lambda(i+1)} - V_{\lambda(i)})/RT \right] \rangle_{\lambda(i).} \quad (3)$$

Here, G_0 and G_1 are the free energies of states 0 and 1, respectively, $V_{\lambda(i)}$ is the potential energy function for the state represented by $\lambda(i)$, and $\langle\rangle_{\lambda(i)}$ denotes the ensemble average of the enclosed quantity for the state $\lambda(i)$.

Starting from the equilibrated structures obtained from the aforementioned procedure, we performed the production dynamics of perturbation for COX-2 in complex with the inhibitors shown in Figure 3. Each perturbation consisted of 21 windows with 5000 steps of equilibration and 10,000 steps of data collection. In this MD–FEP calculation, a periodic boundary condition was employed in the NPT ensemble at 300 K using Berendsen temperature coupling [70] and at constant pressure (1 atm) with isotropic molecule-based scaling. The SHAKE algorithm [71], with a tolerance of 10^{-6}, was applied to fix all bond lengths involving hydrogen atom. We used a time step of 1 fs and a nonbonded-interaction cutoff radius of 10 Å. The free energies reported in the remainder of this paper always refer to the forward direction, i.e., in the direction from $\lambda = 0$ to $\lambda = 1$. As an estimation of the statistical error, we used half the difference between the absolute values of forward and reverse free energy changes, and the error in $\Delta\Delta G_{\text{bind}}$ is calculated as the square root of the sum of the squares of the individual errors in ΔG_{u} and ΔG_{b}.

Results and discussion

Force field design for heme

We used a general approach to the systematic derivation of potential parameters for metalloproteins to extend the AMBER force field for modeling the heme prothetic group. The method involves geometry optimization of heme in its ferric oxidation state at B3LYP/6-31G* level of theory. Figure 4 displays the structure of a local energy minimum whose input structure was taken from the X-ray structure of COX-2 in complex with the inhibitor SC-558 [13]. As in the crystal structure, the ferric ion has a distorted square planar coordination with respect to four pyrrole moieties of protoporphyrin IX ligand. Interatomic distances associated with the ferric ion compare reasonably well with those in the crystal structure.

It is noteworthy that in the optimized structure the RESP atomic charge of the ferric ion decreases from $+3$ e to $+1.49$ e. On the other hand, the atomic charges of ligand atoms become less negative by about 0.18 e as compared to those of the protoporphyrin IX ligand free of the ferric ion. These changes reflect the redistribution of charges between the ferric ion and its ligand atoms upon formation of the metal complex. We used these newly obtained atomic charges in the free energy simulation because it is well known that the "M^{n+}" model is inadequate for maintaining the

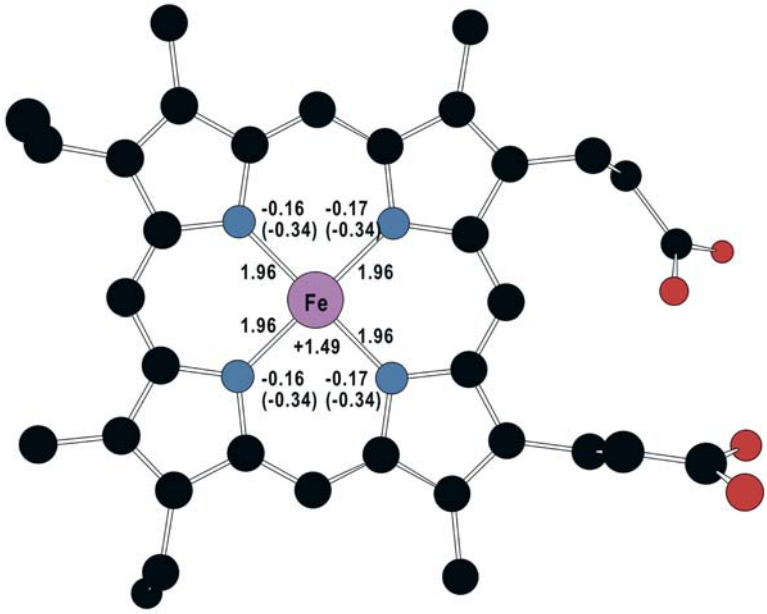

Figure 4. B3LYP/6-31G* optimized structures of the heme in COX-2. The RESP atomic charges (in *e*) and the interatomic distances (in Å) calculated from the optimized structure are indicated. Numbers in parentheses are the RESP atomic charges in the absence of the ferric ion. All hydrogen atoms are omitted for clarity.

coordination geometry in the active sites of metalloenzymes [61, 62].

Docking simulations

Each inhibitor shown in Figure 3 was docked onto the active site of COX-2 from which the inhibitor SC-558 had been removed. Figure 5 shows the lowest-energy AutoDock conformations of diaryl-heterocycle (celecoxib, rofecoxib, valdecoxib, etoricoxib, dup-697) and oxicam (piroxicam and tenoxicam) inhibitors and NS-398. The docking simulation results for structurally related inhibitors are consistent with each other in that the functional groups of similar chemical character are placed in a similar way in the active site. For example, the sulfonyl oxygens of the diaryl-heterocycle inhibitors accept a hydrogen bond from Arg513 and the neighboring phenyl group forms van der Waals contacts with Val523 and Phe518 (Figure 5a). The second aryl group and heterocycles reside in the pocket that involves Arg120, Val349, Tyr355, Leu359, Tyr385, Gly526, Ala527, and Leu531. These structural features are consistent with those in the crystal structure of COX-2 complexed with SC-558 [13]. The binding mode of NS-398 differs from that of diaryl-heterocycle inhibitors in that its sulfonyl oxygen is hydrogen-bonded to Arg120 instead of Arg513 (Figure 5b). As a consequence, the inhibitor nitro group is directed to a small hydrophobic pocket formed by Ala516, Ile517, F518, and Arg513. As in the case of diaryl-heterocycle inhibitors, the phenyl ring of NS-398 establishes a van der Waals contact with Val523. Hence it is seen that the hydrophobic interaction between Val523 and aryl group contributes significantly to the binding of COX-2-selective diaryl-heterocycle inhibitors and NS-398. On the other hand, such an interaction is expected to be unfavorable in the COX-1 active site due to the steric hindrance with the side chain of Ile523 that possesses an additional methyl group at the δ-position.

In contrast to the docking results for six COX-2-selective inhibitors, Val523 is unlikely to contribute significantly to the binding of the two COX-1-selective oxicam inhibitors in the COX-2 active site. For example, the CG2 atom of Val523 resides at a distance of 5–6 Å from the bicyclic rings of both oxicam inhibitors (Figure 5b), forming hydrophobic contacts with the side chains of Leu352, Phe518, and Trp387. Therefore, replacing the valine with isoleucine at residue 523 may lead to the formation of a stable van der

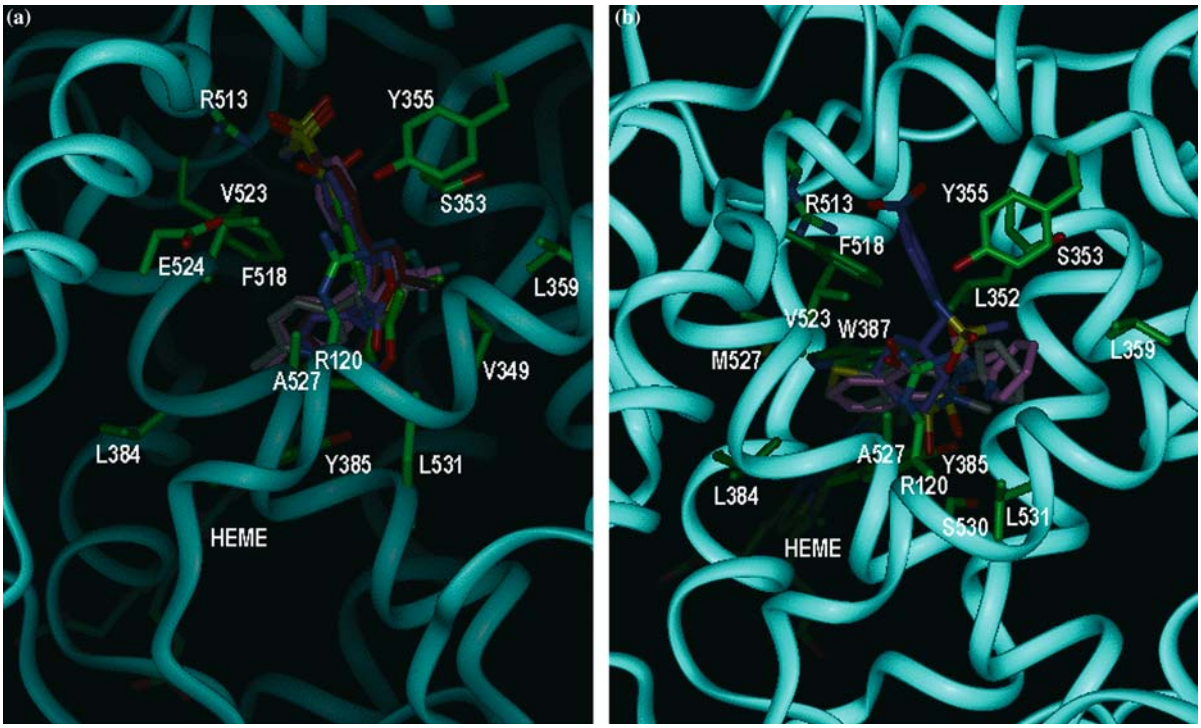

Figure 5. (a) Superimposition of the docked conformations of celecoxib (pink), rofecoxib (violet), DuP-697 (gray), valdecoxib (yellow-green), and etoricoxib (brown). (b) Superimposition of the docked conformations of NS-398 (violet), piroxicam (pink), and tenoxicam (gray).

Waals contact between the additional methyl group at δ-position and the bicyclic ring of the inhibitors. In the structure of COX-2 complexed with the oxicam inhibitors, the roles of hydrogen bond donor for the sulfonyl oxygens are played by the side chains of Tyr385 and Ser530 while the

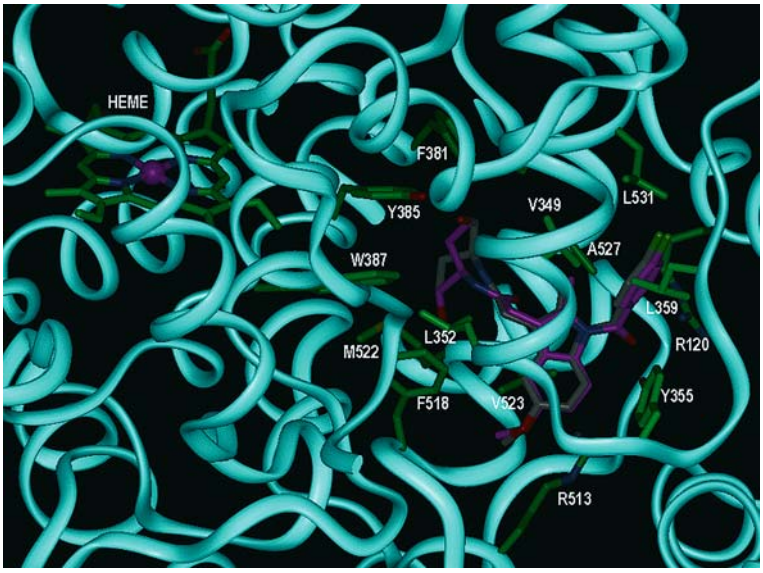

Figure 6. Superimposition of the docked conformations of (*R*)- and (*S*)-enantiomers of an AIE inhibitor in magenta and gray colors, respectively.

inhibitor pyridinyl group is directed to a hydrophobic pocket involving Arg120, Val349, Tyr355, and Leu359.

Figure 6 compares the binding modes of (*R*)- and (*S*)-enantiomers of the AIE inhibitor under investigation. Both enantiomers are stabilized in the COX-2 active site with very similar conformation except for the change of the positions of ethyl and methanol moieties at the chiral center. As a result, the hydroxyl group of (*S*)-enantiomer forms a hydrogen bond with the side chain of Tyr385 whereas that of (*R*)-enantiomer points toward the side chains of Phe518 and Met522. Such a conformational difference between the two enantiomers is the critical factor governing the enantiospecificity in selective inhibition of COX isozymes by the AIE inhibitor, as detailed below.

MD–FEP calculation

To check the reliability of free energy simulations, we examine if the protein structures in the COX-2-inhibitor complexes remain stable under the simulation conditions described in the previous section. For this purpose, we calculated the root-mean-square-deviations from starting structures ($RMSD_{init}$) for all C_α atoms of COX-2. As shown in Figure 7, the $RMSD_{init}$ values remain within 2 Å in most cases with a convergent behavior with respect to the simulation time irrespective of ligand structures, indicating the stability of protein conformation during the entire course of free energy simulations. This result is consistent with the earlier mutagenesis studies, which demonstrated an insignificant effect of the Val $\rightarrow$ Ile mutation at position 523 on the structure and enzymatic catalysis of COX-2 [22, 23]. Therefore, we expect that the calculated free energy differences should be due to the structural perturbations in the side chain of residue 523 and the resulting changes in enzyme–inhibitor interactions instead of some unwanted large conformational changes in the protein (Figure 7).

Summarized in Table 1 are the relative binding free energies ($\Delta\Delta G_{bind}$) of various COX inhibitors in the V523I mutant of COX-2 mimicking COX-1 as compared to those in the wild-type COX-2. We also list the corresponding *in vitro* COX-2 selectivity index (SI) given by the ratio of IC_{50} for COX-1 to that for COX-2. In accordance with the experimental results for the selectivity in COX inhibition, our FEP calculations indicate a decrease in the inhibitory potencies of all five diaryl-heterocycle inhibitors with the change of the side chain at position 523 from valine to isoleucine. In contrast, the COX-1 selective oxicam inhibitors are shown to form more stable enzyme-inhibitor complexes with the V523I mutant of COX-2 than with the wild type. However, we note that the selectivity of NS-398 for COX-2 and that of piroxicam for COX-1 are underestimated within the present framework of FEP calculation, indicating that some modifications should be made in the structural model for COX-1 to improve the accuracy. In this regard, it has been suggested that the residue difference at position 513 between COX-1 (His) and COX-2 (Arg) in the active site may be partially responsible for inhibitor selectivity [13]. This indicates that the double R513H/V523I mutant of COX-2 may be a better structural model for COX-1 than the single V523I mutant. Nonetheless, the overall agreement of the calculated $\Delta\Delta G_{bind}$ value with the selectivity data supports the proposition that the FEP calculations, assuming V523I mutant of COX-2 to be a structural mimic of COX-1, would be a valuable tool for estimating the selectivities of COX inhibitors. The usefulness of the present FEP approach is further exemplified by the results for $\Delta\Delta G_{bind}$ values of the AIE inhibitors, which reveals a significant enantiospecificity in the selective inhibition of COX isozymes. Although the selectivity of (*S*)-AIE is overestimated, the higher value of the calculated $\Delta\Delta G_{bind}$ for (*R*)-AIE than that for (*S*)-AIE by about 2.5 kcal/mol is sufficient to explain the higher selectivity of (*R*)-enantiomer against COX-2 by a factor of 450.

Figure 8 shows the representative MD trajectory snapshots of COX-2 in complex with celecoxib and valdecoxib, both of which possess a sulfonamide moiety as a substituent at one of their two phenyl moieties. It is seen that the sulfonamide nitrogens of the inhibitors donate hydrogen bonds to the side chain aminocarbonyl group of Gln192, and backbone aminocarbonyl oxygens of Leu352 and Ser353. Since the inhibitor phenyl rings with the sulfonamide moiety form a stable van der Waals contact with the side chain of Val523, both inhibitors are expected to reveal different hydrogen-bonding features in the COX-1 active site due to the increased steric hindrance with the side chain of Ile523. As shown in Figure 9, the N–H$\cdots$O

Table 1. Calculated free energy changes in virtual transformations of COX-2 into COX-1 (V523I mutant of COX-2) in the resting (ΔGu) and inhibitor-bound (ΔGb) forms, and relative binding free energies ($\Delta\Delta G_{bind}$) of various COX inhibitors in COX-1 as compared to those in COX-2.

Inhibitors	ΔG_u	ΔG_b	$\Delta\Delta G_{bind}$	SI
COX-2-selective inhibitors				
Celecoxib	−8.9 ± 0.3	−7.8 ± 0.2	1.1 ± 0.4	30
Rofecoxib	−8.9 ± 0.3	−7.9 ± 0.3	1.0 ± 0.4	276
DuP-697	−8.9 ± 0.3	−8.1 ± 0.3	0.8 ± 0.4	80
Valdecoxib	−8.9 ± 0.3	−7.4 ± 0.3	1.5 ± 0.4	261
Etoricoxib	−8.9 ± 0.3	−5.8 ± 0.4	3.1 ± 0.5	344
NS-398	−8.9 ± 0.3	−8.7 ± 0.4	0.2 ± 0.5	>200
(*R*)-AIE	−8.9 ± 0.3	−7.9 ± 0.7	1.0 ± 0.8	590
COX-1-selective or dual inhibitors				
Piroxicam	−8.9 ± 0.3	−9.1 ± 0.3	−0.2 ± 0.4	0.085
Tenoxicam	−8.9 ± 0.3	−10.8 ± 0.2	−1.9 ± 0.4	0.161
(*S*)-AIE	−8.9 ± 0.3	−10.4 ± 0.6	−1.5 ± 0.7	1.300

For comparison, the corresponding *in vitro* COX-2 selectivity index (SI) values of the inhibitors are also listed. All energy values are given in kcal/mol.

hydrogen bond between celecoxib and Gln192 gets weaker as the residue 523 changes from valine to isoleucine: the average N···O distance for the final state (V523I mutant) of free energy simulation is 3.52 Å as compared to the corresponding 2.94 Å for the initial state (wild-type COX-2). Similarly, the N–H···O hydrogen bond between valdecoxib and backbone Ser353 undergoes a weakening or disappears with the transformation of wild-type COX-2 into V523I mutant, which is reflected in lengthening of the average N···O distance from 3.19 Å in the initial state to 3.64 Å in the final state. The changes in the remaining two hydrogen bonds are relatively insignificant with mutual cancellation of their contributions to the inhibitor selectivities. Thus, structural adaptation to the increase in excluded volume at residue 523 leads to the weakening of the hydrogen bonds involving the sulfonamide moiety, and this appears to be a major factor for the selectivity of celecoxib and valdecoxib disfavoring COX-1.

Compared in Figure 10 are the binding modes of rofecoxib in the active sites of wild-type COX-2 and its V523I mutant, which are extracted from trajectory snapshots of MD–FEP simulation of the COX-2-rofecoxib complex. We note that the terminal methyl group of rofecoxib is stabilized in the COX-2 active site through hydrophobic interactions with the side chains of Leu352, Ala516, Ile517, and Phe518. However, in response to the Val → Ile mutation of residue 523, the inhibitor methyl group moves away from the hydrophobic residues and points toward a hydrophilic pocket comprising Gln192, Arg513, and solvent water molecules. This destabilizes the enzyme–inhibitor complex significantly. Because the inhibitor phenyl ring with a sulfoxide moiety stays in close proximity of Val523 in COX-2, an unfavorable steric contact induced by the size-increasing Val → Ile mutation at residue 523 leads to the positional shift of the inhibitor methyl group. Similar structural changes are also observed in the MD–FEP simulations of COX-2 in complexes with DuP-697 and etoricoxib, indicating that the loss of hydrophobic contact of the inhibitor methyl group is responsible for the relatively low activities of these diaryl-heterocycle inhibitors with methyl sulfoxide moiety against COX-1.

Contrasting results are found in the MD–FEP simulation of COX-2 in complex with COX-1-selective oxicam inhibitors. As shown in Figure 11, the Val → Ile mutation at position 523 prevents the side chain of Phe518 from approaching the inhibitor oxicam ring. This leads to a positional shift of the side chain Ser353 in such a way that it forms a hydrogen bond with the inhibitor hydroxyl group. Simultaneously, the backbone aminocarbonyl group at position 523 approaches the amide moiety of the oxicam inhibitor to form a new O···H–N hydrogen bond. Although the hydrogen bond between the side chain of Tyr355 and the inhibitor pyridinyl nitrogen disappears in the final (V523I mutant) state of free energy sim-

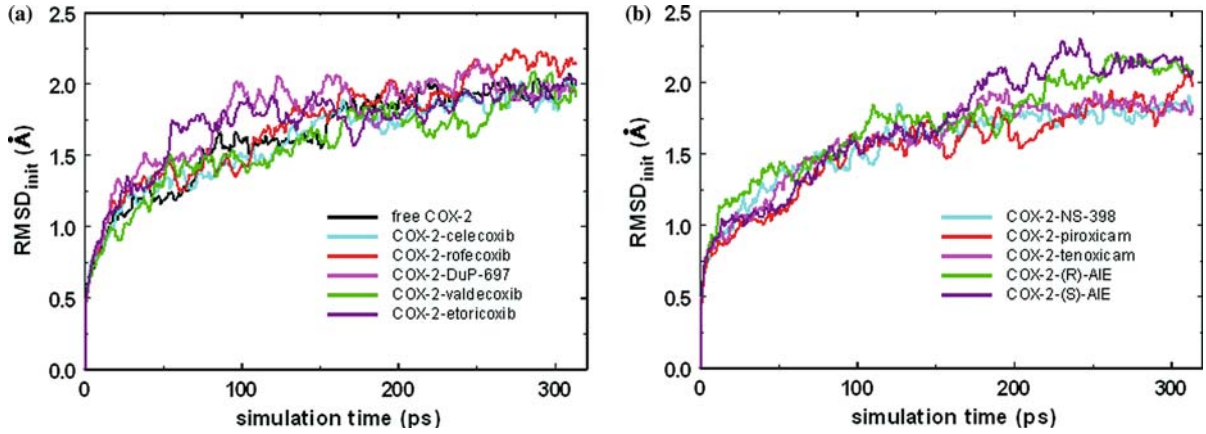

Figure 7. Time dependence of the root mean square deviations from the starting structures ($RMSD_{init}$) for free COX-2 and 10 COX-2-inhibitor complexes under investigation.

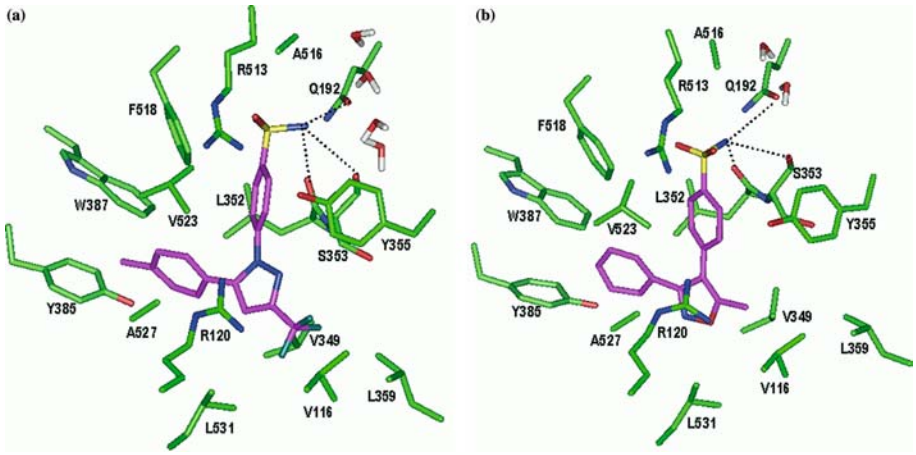

Figure 8. Representative MD trajectory snapshots of (a) COX-2-celecoxib and (b) COX-2-valdecoxib complexes including solvent molecules found near the active site. Each dotted line indicates a hydrogen bond.

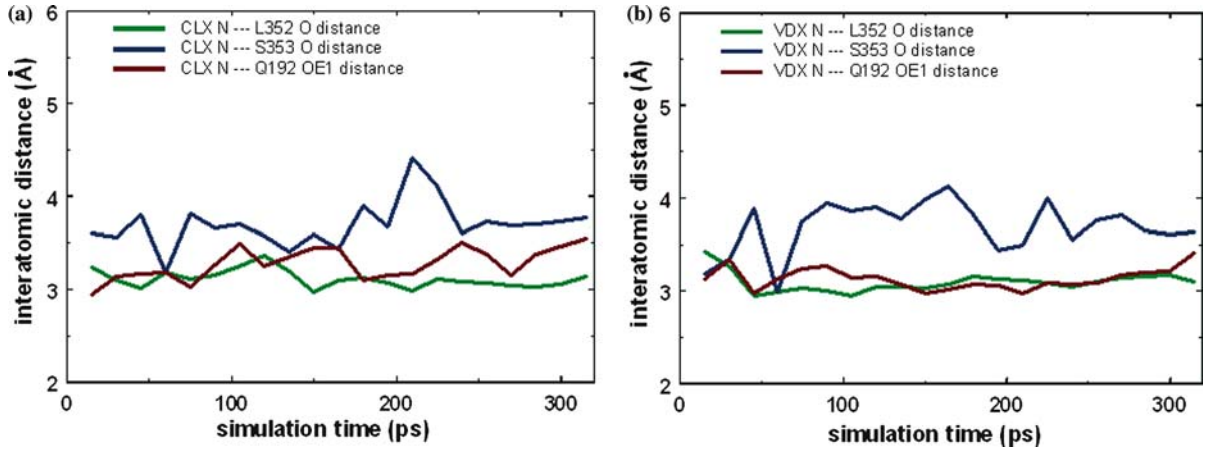

Figure 9. Variation of 15 ps time average of the interatomic distances between the inhibitor sulfonamide nitrogen and hydrogen bond acceptor groups in the COX active site complexed with (a) celecoxib (CLX) and (b) valdecoxib (VDX).

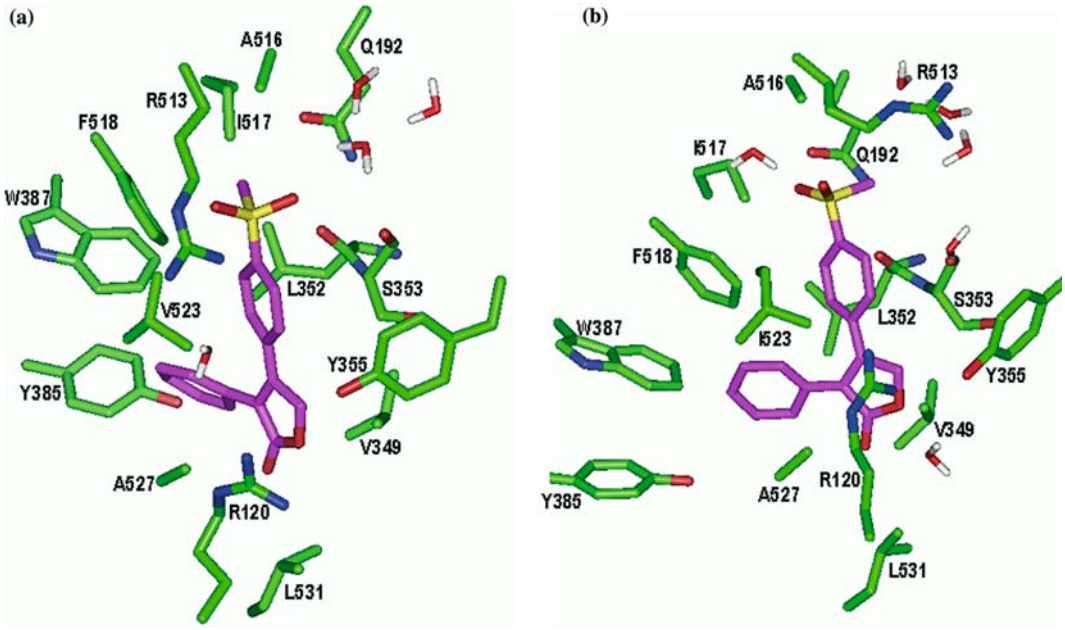

Figure 10. Comparative view of the representative MD trajectory snapshots of COX-2-rofecoxib complex in (a) wild type and (b) V523I mutant states from FEP simulation in solution.

ulation, the formation of two additional hydrogen bonds explains the selectivity of oxicam inhibitors favoring the binding to the COX-1 isozyme.

Now we will address the structural origins of the enantiospecificity in selective COX-2 inhibition by AIE inhibitors. As illustrated in Figure 12, the

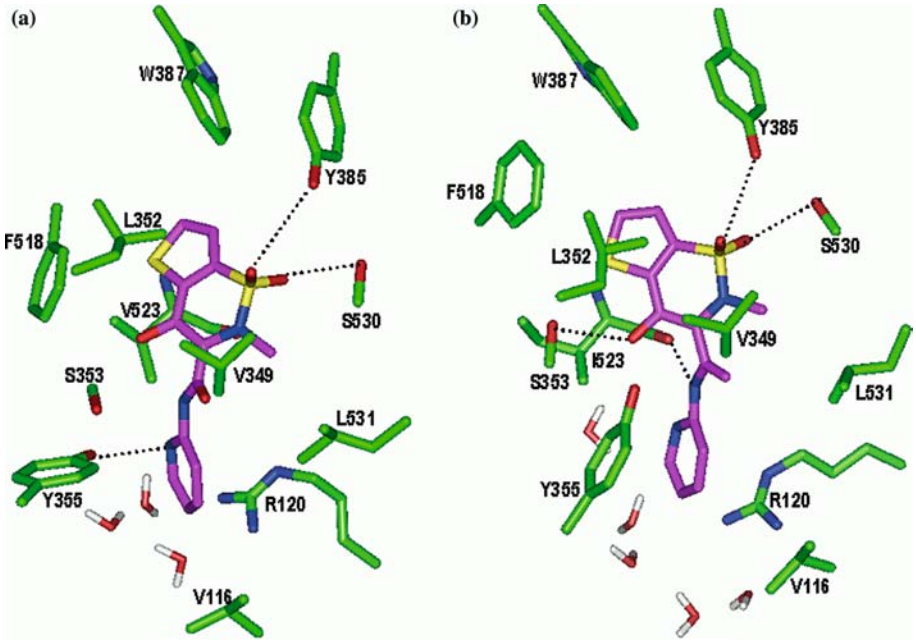

Figure 11. Comparative view of the representative MD trajectory snapshots of COX-2-tenoxicam complex in (a) wild type and (b) V523I mutant states from FEP simulation. Solvent molecules found near the active site are also included. Each dotted line indicates a hydrogen bond.

mutation of Val523 to Ile in COX-2-(R)–AIE complex causes the side chain of Arg513 to separate from the inhibitor methoxy moiety, leading to the rupture of the associated N–H···O hydrogen bond that stabilizes the (*R*)-enantiomer in the COX-2 active site. Apparently, such a movement of Arg513 is due to the steric hindrance with Phe518 that is repelled in response to the increase in excluded volume at position 523. As a consequence of these structural changes, a stable hydrogen bond is established between Arg513 and His90 in the V523I mutant state of simulation. This newly formed hydrogen bond is further stabilized by environmental solvent molecules, which prevents Arg513 from donating a hydrogen bond to the inhibitor methoxy group. Because the rest of enzyme–inhibitor interactions are shown to undergo an insignificant change during the course

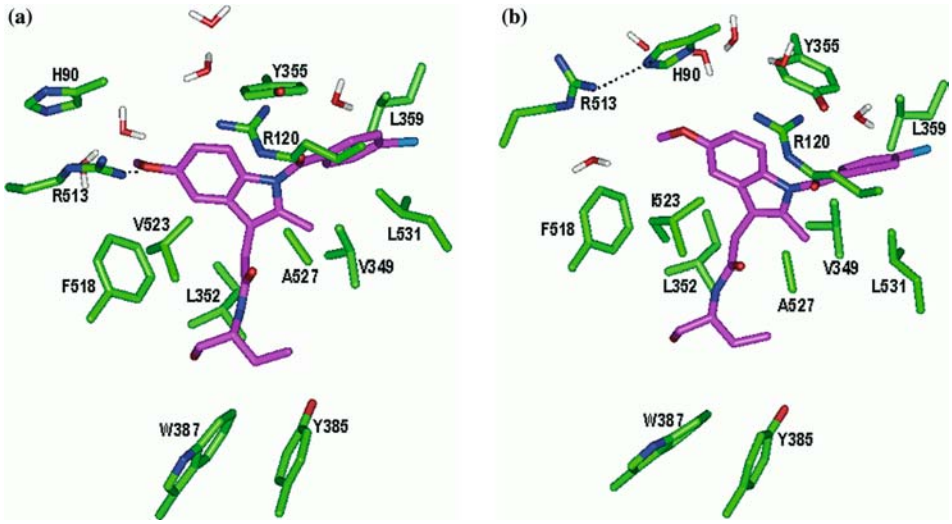

Figure 12. Comparative view of the representative MD trajectory snapshots of COX-2-(*R*)–AIE complex in (a) wild type and (b) V523I mutant states from FEP simulation, including solvent molecules found near the active site. The dotted line indicates a hydrogen bond.

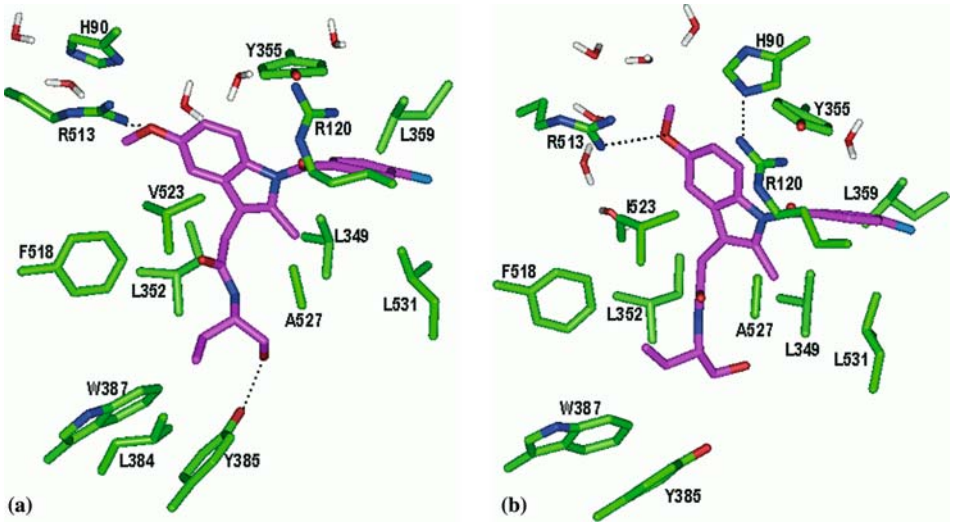

Figure 13. Comparative view of the representative MD trajectory snapshots of COX-2-(*S*)–AIE complex in (a) wild type and (b) V523I mutant states of FEP simulation, including solvent molecules found near the active site. Each dotted line indicates a hydrogen bond.

of MD–FEP simulation, the high selectivity of (*R*)-AIE inhibitor disfavoring COX-1 may be attributed to the disappearance of the hydrogen bond in the COX-1 active site.

Figure 13 compares the binding modes of the (*S*)-AIE inhibitor in the initial and the final states of MD–FEP simulation. It is interesting that in response to the increase in excluded volume at position 523 due to the Val $\rightarrow$ Ile mutation, the side chain of Phe518 in COX-2-(*S*)–AIE complex moves in the opposite longitudinal direction when compared to its motion in COX-2 complexed with the (*R*)-enantiomer. Therefore, the side chain of Arg513 undergoes an insignificant positional shift owing to the lack of steric hindrance with the Phe518. The hydrogen bond between Arg513 and the inhibitor methoxy moiety in the initial COX-2-(*S*)-AIE complex is thus maintained in the final V523I mutant state. In this structure, Arg120 plays the role of hydrogen bond donor with respect to the sidechain of His90 that is repelled as a consequence of the conformational adjustment of (*S*)-AIE to the mutation at Val523. For the same reason, the hydrogen bond between Tyr385 and the inhibitor methanol moiety disappears in the final state of free energy simulation.

The dependence of the mutation-induced positional shift of Phe518 on the inhibitor stereochemisty stems from the different binding modes of the two terminal groups attached to the stereocenter. In the COX-2-(*S*)–AIE complex, the phenyl ring of Phe518 is situated in the vicinity of the terminal ethyl group of the inhibitor with associated interatomic distance of 5–6 Å. Such a positional proximity between the two hydrophobic groups offers the possibility of forming a stable van der Waals contact when Phe518 is repelled by the newly formed methyl group at residue 523. Indeed, as can be seen in Figure 13b, the ethyl moiety is bound in the hydrophobic pocket consisting of Leu352, Trp387, and Phe518 in the V523I mutant state. Considering the fact that the (*S*)-enantiomer are a potent inhibitor for both COX isozymes [56], the establishment of such a stable van der Waals contact is believed to compensate the energy loss caused by the rupture of the hydrogen bond between Tyr385 and the inhibitor hydroxy group. On the other hand, the approach of Phe518 to the stereocenter in the COX-2-(*R*)–AIE complex is prohibited by the hydrophilic methanol moiety of the (*R*)-enantiomer that occupies the same position as the terminal inhibitor ethyl moiety in the COX-2-(*S*)–AIE complex. Thus, the enantiospecificity in selective COX-2 inhibition by the AIE isomers can be attributed to the difference in binding modes of the two terminal groups bonded to the stereocenter.

Conclusions

We have investigated the energetic and structural origins for selective inhibition of COX isozymes by means of the combined computational approach involving docking experiment, force field design for the heme prothetic group, and MD–FEP simulations. Assuming that the V523I mutant of COX-2 is a relevant structural model for COX-1, the present computational strategy proved to be successful in explaining the selectivities of known COX inhibitors for one of the two COX isozymes. For example, the binding affinities of all COX-2-selective inhibitors under consideration were shown to decrease with the change of residue 523 from valine to isoleucine because of the weakening and/or disappearance of hydrogen bond and hydrophobic interactions that stabilize the inhibitors in the COX-2 active site. In contrast, the COX-1-selective oxicam inhibitors gain extra stabilization energy as the receptor changes from COX-2 to COX-1 due to the formations of new hydrogen bonds in the enzyme-inhibitor complexes. The utility of the combined computational approach is further exemplified in identifying the energetic and structural basis for the stereospecificity of selective COX-2 inhibition by α-substituted indomethacin ethanolamide inhibitors. The predicted differential binding mode of each inhibitor in the two COX isoforms is expected to provide useful information for the rational design of new COX-2-selective inhibitors.

Acknowledgements

This work was supported by Grant No. R02-2002-000-00006-0 from the Basic Research Programs of the Korea Science and Engineering Foundation. The authors would also like to acknowledge the support from KISTI (Korea Institute of Science and Technology Information) under ''The Sixth Strategic Supercomputing Support Program'' with

Dr. Sang Min Lee as the technical supporter. The use of the computing system of the Supercomputing Center is also greatly appreciated.

References

1. Smith, W.L., DeWitt, D.L. and Garavito, R.M., Annu. Rev. Biochem., 69 (2000) 145.
2. Rouzer, C.A. and Marnett, L.J., Chem. Rev., 103 (2003) 2239, and references therein.
3. FitzGerald, G.A., Nat. Rev. Drug Discov., 2 (2003) 879.
4. Shiff, S.J., Shivaprasad, P. and Santini, D.L., Curr. Opin. Pharmacol., 3 (2003) 352.
5. Kalgutkar, A.S. and Zhao, Z., Curr. Drug Targets, 2 (2001) 79.
6. Moore, B.C. and Simmons, D.L., Curr. Med. Chem., 7 (2000) 1131.
7. Song, X., Lin, H.-P., Johnson, A.J., Tseng, P.-H., Yang, Y.-T., Kulp, S. K. and Chen, C.-S., J. Natl. Cancer Inst., 94 (2002) 585.
8. Crofford, L.J., Lipsky, P.E., Brooks, P., Abramson, S.B., Simon, L.S. and van de Putte, L.B., Arthritis Rheum., 43 (2000) 4.
9. Weggen, S., Eriksen, J.L., Das, P., Sagi, S.A., Wang, R., Pietrzik, C.U., Findlay, K.A., Smith, T.E., Murphy, M.P., Bulter, T., Kang, D.E., Marquez-Sterling, N., Golde, T.E. and Koo, E.H., Nature, 414 (2001) 212.
10. Zhou, Y., Su, Y., Li, B., Liu, F., Ryder, J.W., Wu, X., Gonzalez-DeWhitt, P.A., Gelfanova, V., Hale, J.E., May, P.C., Paul, S.M. and Ni, B., Science, 302 (2003) 1215.
11. Picot, D., Loll, P.J. and Garavito, R.M., Nature, 367 (1994) 243.
12. Loll, P.J., Picot, D. and Garavito, R.M., Nat. Struct. Biol., 2 (1995) 637.
13. Kurumbail, R.G., Stevens, A.M., Gierse, J.K., McDonald, J.J., Stegeman, R.A., Pak, J.Y., Gildehaus, D., Miyashiro, J.M., Penning, T.D., Seibert, K., Isakson, P.C. and Stallings, W.C., Nature, 384 (1996) 644.
14. Kiefer, J.R., Pawlitz, J.L., Moreland, K.T., Stegeman, R.A., Hood, W.F., Gierse, J.K., Stevens, A.M., Goodwin, D.C., Rowlinson, S.W., Marnett, L.J., Stallings, W.C. and Kurumbail, R.G., Nature, 405 (2000) 97.
15. Malkowski, M.G., Ginell, S.L., Smith, W.L. and Garavito, R.M., Science, 289 (2000) 1933.
16. Thuresson, E.D., Malkowski, M.G., Lakkides, K.M., Rieke, C.J., Mulichak, A.M., Ginell, S. L., Garavito, R.M. and Smith, W.L., J. Biol. Chem., 276 (2001) 10358.
17. Malkowski, M.G., Thuresson, E.D., Lakkides, K.M., Rieke, C.J., Micielli, R., Smith, W.L. and Garavito, R.M., J. Biol. Chem., 276 (2001) 37547.
18. Loll, P.J., Picot, D., Ekabo, O. and Garavito, R.M., Biochemistry, 35 (1996) 7330.
19. Selinsky, B.S., Gupta, K., Sharkey, C.T. and Loll, P.J., Biochemistry, 40 (2001) 5172.
20. Garavito, R.M. and Mulichak, A.M., Annu. Rev. Biophys. Biomol. Struct., 32 (2003) 183.
21. Following the conventional numbering scheme established to aid convenience of structural and functional comparisons across species, the residues of COXs are numbered to correspond to the ovine COX-1 sequence.
22. Gierse, J.K., McDonald, J.J., Hauser, S.D., Rangwala, S.H., Koboldt, C.M. and Seibert, K., J. Biol. Chem., 271 (1996) 15810.
23. Guo, Q., Wang, L.-H., Ruan, K.-H. and Kulmacz, R.J., J. Biol. Chem., 271 (1996) 19134.
24. Wong, E., Bayly, C., Waterman, H.L., Riendeau, D. and Mancini, J.A., J. Biol. Chem., 272 (1997) 9280.
25. Dannhardt, G. and Kiefer, W., Eur. J. Med. Chem., 36 (2001) 109.
26. Kalgutkar, A.S., Exp. Opin. Ther. Pat., 9 (1999) 831.
27. DeWitt, D.L., Mol. Pharmacol., 55 (1999) 625.
28. Marnett, L.J. and Kalgutkar, A.S., Curr. Opin. Chem. Biol., 2 (1998) 482.
29. Shin, S.S., Byun, Y., Lim, K.M., Choi, J.K., Lee, K.-W., Moh, J.H., Kim, J.K., Jeong, Y.S., Kim, J.Y., Choi, Y.H., Koh, H.-J., Park, Y.-H., Oh, Y.I., Noh, M.-S. and Chung, S., J. Med. Chem., 47 (2004) 792.
30. Baruah, B., Dasu, K., Vaitilingam, B., Vanguri, A., Casturi, S.R. and Yeleswarapu, K.R., Bioorg. Med. Chem. Lett., 14 (2004) 445.
31. Uddin, M.J., Rao, P.N.P. and Knaus, E.E., Bioorg. Med. Chem., 11 (2003) 5273.
32. Praveen Rao, P.N., Amini, M., Li, H., Habeeb, A.G. and Knaus, E.E., J. Med. Chem., 46 (2003) 4872.
33. Rao, P.N.P., Amini, M., Li, H., Habeeb, A.G. and Knaus, E.E., Bioorg. Med. Chem. Lett., 13 (2003) 2205.
34. Khanapure, S.P., Garvey, D.S., Young, D.V., Ezawa, M., Earl, R.A., Gaston, R.D., Fang, X., Murty, M., Martino, A., Shumway, M., Trocha, M., Marek, P., Tam, S.W., Janero, D.R. and Letts, L.G., J. Med. Chem., 46 (2003) 5484.
35. Black, W.C., Brideau, C., Chan, C.-C., Charleson, S., Cromlish, W., Gordon, R., Grimm, E.L., Hughes, G., Leger, S., Li, C.-S., Riendeau, D., Thérien, M., Wang, Z., Xu, L.-J. and Prasit, P., Bioorg. Med. Chem. Lett., 13 (2003) 1195.
36. Joo, Y.H., Kim, J.K., Kang, S.-H., Noh, M.-S., Ha, J.-Y., Choi, J. K., Lim, K.M., Lee, C.H. and Chung, S., Bioorg. Med. Chem. Lett., 13 (2003) 413.
37. Li, C.S., Brideau, C., Chan, C.C., Savoie, C., Claveau, D., Charleson, S., Gordon, R., Greig, G., Gauthier, J.Y., Lau, C.K., Riendeau, D., Thérien, M., Wong, E. and Prasit, P., Bioorg. Med. Chem. Lett., 13 (2003) 597.
38. Paramashivappa, R., Kumar, P.P., Rao, P.V.S. and Rao, A.S., Bioorg. Med. Chem. Lett., 13 (2003) 657.
39. Park, C.H., Siomboing, X., Yous, S., Gressier, B., Luyckx, M. and Chavatte, P., Eur. J. Med. Chem., 37 (2002) 461.
40. Palomer, A., Cabre, F., Pascual, J., Campos, J., Trujillo, M.A., Entrena, A., Gallo, M.A., Garcia, L., Mauleon, D. and Espinosa, A., J. Med. Chem., 45 (2002) 1402.
41. Hashimoto, H., Imamura, K., Haruta, J. and Wakitani, K., J. Med. Chem., 45 (2002) 1511.
42. Noguchi, T., Shimazawa, R., Nagasawa, K. and Hashimoto, Y., Bioorg. Med. Chem. Lett., 12 (2002) 1043.
43. Kalgutkar, A.S., Rowlinson, S.W., Crews, B.C. and Marnett, L.J., Bioorg. Med. Chem. Lett., 12 (2002) 521.
44. Liu, H.X., Zhang, R.S., Yao, X.J., Liu, M.C., Hu, Z.D. and Fan, B.T., J. Comput.-Aided Mol. Des., 18 (2004) 389.
45. Garg, R., Kurup, A., Mekapati, S.B. and Hansch, C., Chem. Rev., 103 (2003) 703.
46. Price, M.L.P. and Jorgensen, W.L., J. Am. Chem. Soc., 122 (2000) 9455.

47. Price, M.L.P. and Jorgensen, W.L., Bioorg. Med. Chem. Lett., 11 (2001) 1541.
48. Soliva, R., Almansa, C., Kalko, S.G., Luque, F.J. and Orozco, M., J. Med. Chem., 46 (2003) 1372.
49. Garcia-Nieto, R., Perez, C. and Gago, F., J. Comput.-Aided Mol. Des., 14 (2000) 147.
50. Chavatte, P., Yous, S., Marot, C., Baurin, N. and Lesieur, D., J. Med. Chem., 44 (2001) 3223.
51. Filizola, M., Perez, J.J. and Palomer, J.J., Mauleon, D., J. Mol. Graph. Model., 15 (1997) 290.
52. Llorens, O., Perez, J.J., Palomer, A. and Mauleon, D., J. Mol. Graph. Model., 20 (2002) 359.
53. Desiraju, G.R., Sarma, J.A.R.P., Raveendra, D., Gopalakrishnan, B., Thilagavathi, R., Sobhia, M.E. and Subramanya, H.S., J. Phys. Org. Chem., 14 (2001) 481.
54. Marot, C., Chavatte, P., Lesieur, D., Quant. Struct.-Act. Relat., 19 (2000) 127.
55. Ruiz, J., Pérez, C. and Pouplana, R., Bioorg. Med. Chem., 11 (2003) 4207.
56. Kozak, K.R., Prusakiewicz, J.J., Rowlinson, S.W. and Marnett, L.J., Bioorg. Med. Chem. Lett., 12 (2002) 1315.
57. Morris, G.M., Goodsell, D.S., Halliday, R.S., Huey, R., Hart, W.E., Belew, R.K. and Olson, A.J., J. Comput. Chem., 19 (1998) 1639.
58. Mehler, E.L. and Solmajer, T., Protein Eng, 4 (1991) 903.
59. Stouten, P.F.W., Frömmel, C., Nakamura, H. and Sander, C., Mol. Simul., 10 (1993) 97.
60. Hoops, S.C., Anderson, K.W. and Merz, K.M., Jr., J. Am. Chem. Soc., 113 (1991) 8262.
61. Stote, R.H. and Karplus, M., Proteins: Struct. Funct. Genet., 23 (1995) 12.
62. Toba, S., Colombo, G. and Merz, K.M., Jr., J. Am. Chem. Soc., 121 (1999) 2290.
63. Ringnalda, M.N., Jaguar, Schroedinger, Inc., Portland, OR, 1997.
64. Giammona, D.A. Ph.D. thesis, University of California, Davis, CA, 1984.
65. Bayly, C.A., Cieplak, P., Cornell, W.D. and Kollman, P.A., J. Phys. Chem., 97 (1993) 10269.
66. Cornell, W.D., Cieplak, P., Bayly, C.I., Gould, I.R., Merz, K.M., Jr., Ferguson, D.M., Spellmeyer, D.C., Fox, T., Caldwell, J.W. and Kollman, P.A., J. Am. Chem. Soc., 117 (1995) 5179.
67. Case, D.A., Pearlman, D.A., Caldwell, J.W., Cheatham, T.E., III, Ross, W.S., Simmerling, C., Darden, T., Merz, K.M., Jr., Stanton, R.V., Cheng, A., Vincent, J.J., Crowley, M., Tsui, V., Radmer, R., Duan, Y., Pitera, J., Massova, I., Seibel, G.L., Singh, U.C., Weiner, P. and Kollman, P.A., AMBER 7, University of California, San Francisco, CA, 2002.
68. Jorgensen, W.L., Chandrasekhar, J., Madura, J.D., Impey, R.W. and Klein, M.L., J. Chem. Phys., 79 (1983) 926.
69. Zwanzig, R.J., J. Chem. Phys., 22 (1954) 1420.
70. Berendsen, H.C., Postma, J.P.M., van Gunsteren, W.F., DiNola, A. and Haak, J.R., J. Chem. Phys., 81 (1984) 3684.
71. Ryckaert, J.P., Ciccotti, G. and Berendsen, H.C., J. Comput. Phys., 23 (1977) 327.